Int J Mech Mater Des
https://doi.org/10.1007/s10999-023-09703-3

Development of a novel testing concept for combined characterisation of tensile and compressive properties

Timo Bensing · Martin Moneke

Received: 30 August 2023 / Accepted: 21 December 2023

Abstract A novel material testing concept is developed in order to provide tensile and compressive properties within a single mechanical test. A new specimen geometry is designed for testing in a universal testing machine. Under tensile load, both a homogeneous tensile stress condition as well as a homogeneous compressive stress condition occur in the specimen. Measurements accompanying the experimental test with digital image correlation provide tensile and compressive Poisson's ratio as well as tensile modulus. These properties are input parameters for subsequent finite element simulations. The compressive modulus is determined by iteratively adjusting finite element simulations in order to couple experimental and simulated results. For validating the concept, experimental tests are carried out on polyoxymethylene. While the tensile Poisson's ratio of the new concept shows the best agreement with the reference value, the compressive modulus is approximately 15% higher. Further work should focus on an appropriate material model in order to reduce the deviation.

Keywords Polymers · Digital image correlation · Finite element simulation · Tension · Compression · Combined characterisation

T. Bensing · M. Moneke (✉)
Institute of Plastics Engineering, Darmstadt University of Applied Sciences, Darmstadt, Germany
e-mail: martin.moneke@h-da.de

1 Introduction

Digital image correlation (DIC) is used as a technique to measure displacement and deformation of surface areas. It has been applied in a variety of fields in the past. One of the main applications is detecting and monitoring cracks in different kinds of building materials. Besides detecting crack initiation (Lin and Labuz 2013; Navaratnam et al. 2020; Liu et al. 2021) and investigating the fracture process zone (Miao et al. 2020; Moazzami et al. 2020; Skarżyński 2020), the crack growth is of interest (Abanto-Bueno and Lambros 2002; Navaratnam et al. 2020). Mostly, building materials are tested in three-point or four-point bending tests (Lin and Labuz 2013; Miao et al. 2020; Navaratnam et al. 2020). DIC is also suited for high-temperature measurements (Bing et al. 2009; Grant et al. 2009; Pan et al. 2020) up to 3000 °C (Pan et al. 2020) or vibration measurements (Helfrick et al. 2011; Ngeljaratan and Moustafa 2020). Field applications range from vibration frequency measurement of footbridges (Ngeljaratan and Moustafa 2020) to landslide monitoring for tracking ground displacements (Mazzanti et al. 2020). One of the most substantial features is the local strain measurement. It can support standard tensile tests, e.g. by providing local strain data in order to determine the true stress strain curve (Grytten et al. 2009). Overall, DIC has been established as a reliable and highly precise technique for non-contact and local deformation measurement.

Published online: 19 January 2024

Until today many researchers carry out mechanical tests according to the test standards ASTM D638/ISO 527 and ASTM D695/ISO 604 (e.g. Ali et al. 2022; Chaitat et al. 2022; Kananathan et al. 2022; Mutyala et al. 2022; Rudawska and Frigione 2022). Consequently, they need to perform separate tests to determine tensile and compressive properties. Some researchers attempt to receive tensile and compressive properties within a single test. Mujika et al. (2006) performed bending tests with strain gauges attached to the tensile and compressive side of the specimen. By using the ratio of measured tensile and compressive strain and an analytical approach, they derived tensile and compressive moduli. Kim et al. (2011) used the bending modulus of structural lumber to predict its tensile and compressive moduli by performing a regression analysis. Røhl et al. (1991) investigated the tensile and compressive behaviour of cancellous, human bones and received both tensile and compressive moduli from the same specimen by consecutive loading under tension and compression.

Several approaches have been made where a combination of a full-field measurement technique like DIC and additional FE simulations is used to determine material parameters. The strains measured in the experiment are coupled to the simulated strain field of FE simulations. The material parameters are iteratively updated until the simulated and experimental results match. This procedure is called finite element model updating method (Avril et al. 2008). Doing so, Lecompte et al. (2007) carried out biaxial tensile tests on cruciform specimen of glass fibre reinforced epoxy in order to get the in-plane orthotropic material parameters. Pottier et al. (2011) used thin aluminium sheets similar to standard tensile test specimens with and without a hole as well as sheets with an occurring shear stress to gain anisotropic elastic–plastic material parameters. A similar approach is followed by Molimard et al. (2005) who performed an open-hole tensile test on composite materials in order to get the four in-plane orthotropic material parameters. He et al. (2016) gained tensile and compressive moduli among other parameters with a short-beam shear test on a fibre reinforced composite.

Following a similar approach this work aims to develop a novel mechanical testing concept for a combined characterisation of Young's modulus and Poisson's ratio for both, tension and compression stress states. Therefore, a new specimen geometry is designed that is tested in a universal testing machine. Furthermore, a finite element model updating method is developed and implemented to receive the four constitutive parameters.

Instead of performing two separate standard tests according to ISO 527 and ISO 604, the new concept enables the characterisation of elastic tensile and compressive properties in a single test. Furthermore, the new concept provides a more robust determination of the compressive properties since the typical, non-uniform compressive load at the beginning of the standard compressive test does not occur. Therefore, a time-consuming review and post-processing of the results is avoided. Overall, this approach can save time and resources in fields of activity like component design or material development.

2 Materials and methods

2.1 Materials

For the validation of the new testing concept, experimental tests have been performed on the thermoplastic polymer poly (oxy methylene) (POM). The copolymer Hostaform® C 9021 from the manufacturer Celanese has been provided in the form of granulate. It is characterised as a material with a low moisture absorption as well as a good chemical resistance and it does not contain any fillers. The raw material was injection moulded into plates with a length of 150 mm, a width of 100 mm and a thickness of 3 mm. Afterwards, the required test specimens were milled out of the plates. Milling out of plates was chosen as the manufacturing process because in this case there is no need for acquiring new tools during the development process and it provides the possibility of flexibly adjusting or optimising the specimen geometry. Before testing, the specimens had been conditioned at a temperature of (23 ± 2) °C and a relative humidity of (50 ± 10) % for at least 16 h according to ISO 29988-2. Conditioning the specimens is done in order to reduce environmental influences during testing and for a better comparability of the testing results. After conditioning the tests were immediately carried out in a room without climate control and a temperature close to 23 °C.

2.2 Specimen types

Three types of specimens for mechanical tests were designed. First, there is a combined tensile compressive test specimen for the new testing concept that has a unique design, see Fig. 1 (bottom). Next, there are tensile and compressive test specimens for the validation of the new testing concept. The shape of the tensile test specimen is similar to the type 1A according to ISO 527-2 but with a total length of 100 mm, a shoulder length of 20 mm and a parallel length of 37.5 mm, see Fig. 1 (top). The compressive test specimen is cut out of the injection moulded plates perpendicular to the melt flow direction and has a length of 20 mm, a width of 10 mm and a thickness of 3 mm.

2.3 Tensile and compressive tests

The quasi-static mechanical tests were carried out with a ZwickRoell Universal Testing Machine AllroundLine Z100, see Fig. 2. The load cell used is the Xforce HP 10 kN. The crosshead speed differs depending on the specimen type. The tests were performed without preloading.

Wedge screw grips (type 8306) were used for the tensile tests where the closing force is adjusted via a handwheel. In order to establish a uniform closing force a torque of 20 Nm has been applied with a torque wrench. Circular compression platens with a diameter of 136 mm were used for the compressive tests. The platens were adjusted plane-parallel prior testing.

The Poisson's ratios of all specimens were measured by DIC. Due to manufacturing tolerances of the compressive test specimen the stress strain diagram starts with a sag which cannot be attributed to a material phenomenon. Therefore, the measurement results were post-processed using Python. In order to receive a degressive stress strain curve the largest incline is detected and the sag prior this

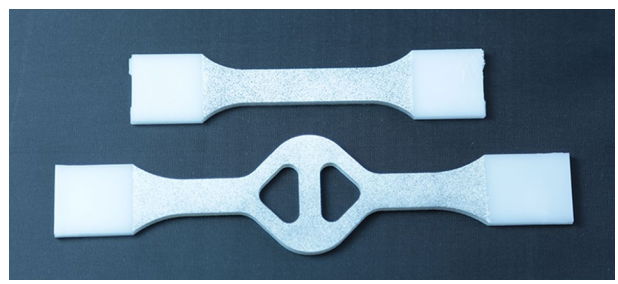

Fig. 1 Tensile test specimen (top) and combined tensile compressive test specimen (bottom)

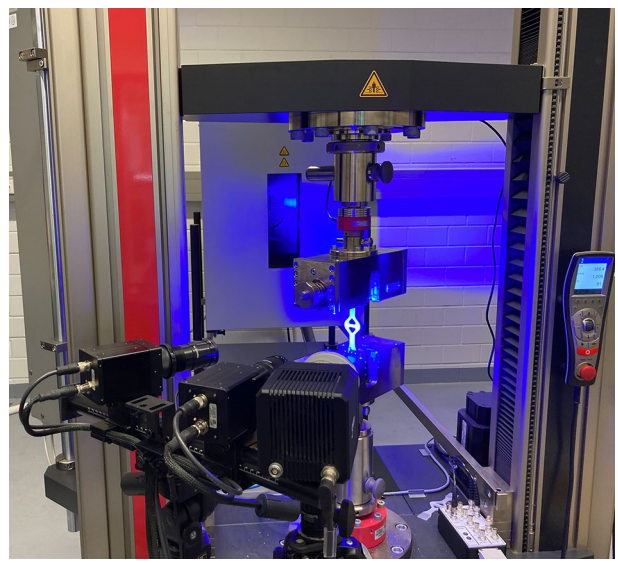

Fig. 2 DIC measurement setup for tensile tests equipped with a combined tensile compressive test specimen

point is replaced by a straight line with this very incline.

2.4 Digital image correlation

GOM Aramis Adjustable SRX was used as the device for DIC. Two cameras were installed for three-dimensional deformation measurement with 12 MP cameras and lenses of type Titaner B 75 mm each. The camera angle was set to 25°. The measuring volume had a height of 85 mm, a width of 65 mm and a depth of 45 mm with a measuring distance of 427 mm. The specimen surfaces were sprayed with a water-based paint spray for a uniform white primer coat prior testing. After priming, the speckle pattern was applied with a graphite paint spray. The chosen facet size is 19 to 19 pixels with a facet step of 16 pixels. The measuring frequency and shutter time were adjusted for each specimen type. The measured values of the universal testing machine, load and movement, were transmitted to the DIC software (Aramis Professional 2020) during testing in order to get synchronised data for the evaluation.

2.5 FE simulation

FE simulations were carried out on the combined tensile compressive test specimen using Abaqus as the solver. A linear elastic material model with Young's modulus and Poisson's ratio was implemented. The element type used is C3D20.

3 Results and discussion

3.1 Testing concept

The objective of the new testing concept is to gain tensile and compressive properties by a specimen that is tested in a universal testing machine. The desired properties are Young's modulus as well as Poisson's ratio for tension and compression. For this purpose, a unique specimen geometry is developed which can be seen in Fig. 3.

When clamping the specimen into the testing machine and applying a tensile force three areas with a homogeneous stress condition will occur: two areas with a tensile stress at the top and the bottom ('T1' and 'T2') as well as one area with a compressive stress in the beam at the centre of the specimen ('C'). Two tensile areas are defined and used because of the dependence of the material behaviour on the flow path of the melt which coincides with the y-axis. The homogeneous compression is induced due to stretching the bars of the diamond-shaped middle part.

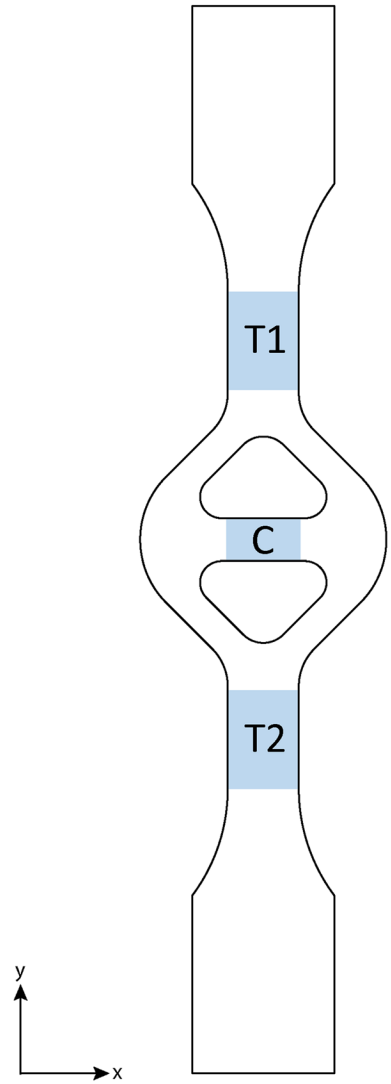

Fig. 3 Design of the combined tensile compressive test specimen in which homogeneous tensile stress conditions (T1, T2) and a homogeneous compressive stress condition (C) occur after loading along the y-axis

The test is done with a crosshead speed of 1 mm/min. From the test, tensile modulus (E_T) and Poisson's ratio (ν_T and ν_C) of tension and compression both can be obtained using Eqs. 1, 2, 3

$$E_T = \frac{\Delta\left(\frac{\sigma_y^{T1}+\sigma_y^{T2}}{2}\right)}{\Delta\left(\frac{\varepsilon_y^{T1}+\varepsilon_y^{T2}}{2}\right)} \tag{1}$$

$$\nu_T = -\frac{\Delta\left(\frac{\varepsilon_x^{T1}+\varepsilon_x^{T2}}{2}\right)}{\Delta\left(\frac{\varepsilon_y^{T1}+\varepsilon_y^{T2}}{2}\right)} \tag{2}$$

$$\nu_C = -\frac{\Delta\varepsilon_y^C}{\Delta\varepsilon_x^C} \tag{3}$$

The tensile and compressive strains of all three areas (ε_x^T, ε_y^T, ε_x^C and ε_y^C) are measured separately using local DIC data. The tensile stress (σ_y^T) of both tensile areas results from the applied force divided by the respective cross section. All of the three parameters are calculated in a strain range between 0.05% and 0.25% according to ISO 527-1 using linear regression.

Using the measurement data from the universal testing machine and the DIC system only, the compressive modulus cannot be derived. Additional information about the stress condition in the compressive area is needed. For determining the compressive modulus, subsequent FE simulations are carried out. Due to the three symmetry planes of the specimen perpendicular to each spatial coordinate, a CAD model with an eighth of the volume of the specimen is realised which is shown in Fig. 4.

The tensile load is implemented as a constant movement of the shoulder by 0.5 mm, making a total movement of 1 mm due to the symmetry of the model. Two linear elastic material models are implemented, one for the tensile behaviour and one for the compressive behaviour. The compressive properties are implemented in the compressive area marked green in Fig. 4a. For the remaining sections of the specimen only the tensile properties are attributed to the elements. The strain and stress data are evaluated in the area marked red for the tensile behaviour and in the area marked green for the compressive behaviour in Fig. 4b. The evaluated compressive area is smaller in order to exclude peak values in the transition area of the two material models. Finally, the compressive modulus is the result of an optimisation loop with several FE simulations following the procedure shown in Fig. 5.

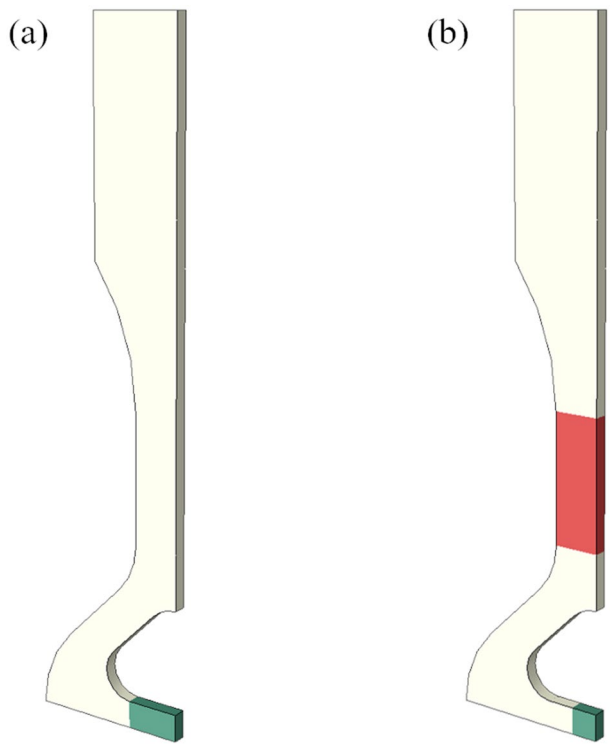

Fig. 4 CAD model of the combined tensile compressive test specimen with the eighth volume for the FE analysis where **a** compressive properties are attributed to the area marked green and tensile properties in the remaining specimen and **b** tensile stress and strain are evaluated in the area marked red with at the same time compressive stress and strain in the area marked green

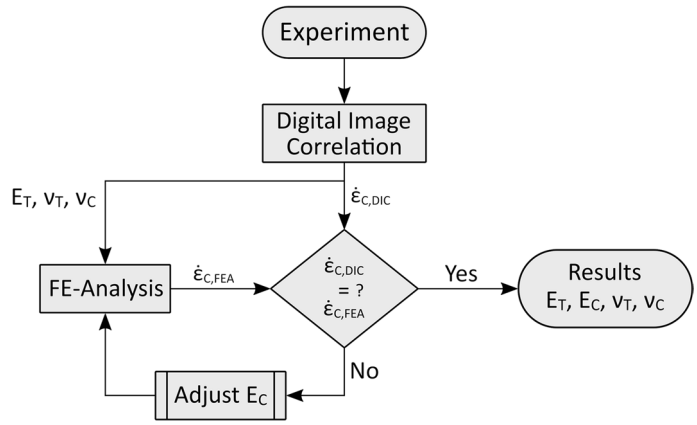

Fig. 5 Optimisation loop using FE simulations for gaining the compressive modulus with input parameters from the tensile test

As mentioned above, the experiment using DIC provides both Poisson's ratios (ν_T and ν_C) as well as the tensile modulus (E_T). All three properties are fixed input parameters for the FE analysis. For the initial FE simulation, the compressive modulus (E_C) is set equal to the tensile modulus. In the next step, the resulting strain rate in the compressive area of the simulation ($\dot{\varepsilon}_{C,FEA}$) is compared to the one of the experiment measured by DIC ($\dot{\varepsilon}_{C,DIC}$). If the strain rate of the simulation is lower, the compressive modulus will be reduced for the next run in order to gain a higher strain rate. Following this procedure, the compressive modulus will be adjusted until both strain rates match each other within a defined accuracy for the modulus.

3.2 Specimen geometry optimisation

Relaxation and retardation are characteristic phenomena of polymers. As a result, the material behaviour is particularly time-dependent. Accompanying, the resulting constitutive properties determined with the new testing concept depend on the state of stress and thereby the strain rate within the specimen. The state of stress is influenced by the geometric design of the specimen like the width of the compressive beam in the centre of the specimen (w_3). In order to receive comparable results for tensile and compressive properties, the specimen geometry is adjusted until the tensile and compressive stress levels are in a similar range. The variation parameters are shown in Fig. 6.

The geometry is optimised using FE simulations. A uniform, linear elastic material model is implemented with a Young's modulus of 2400 MPa and a

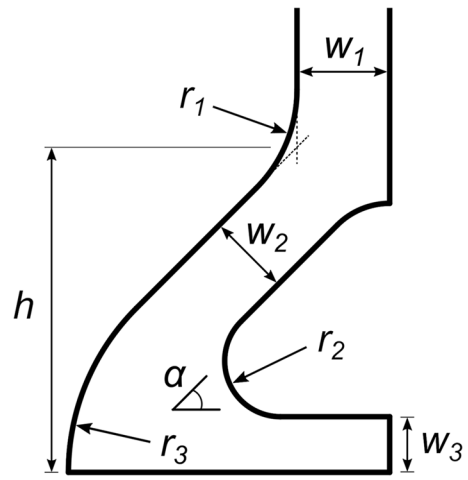

Fig. 6 Variation parameter for the optimisation of the specimen geometry

Poisson's ratio of 0.4. Prior to optimisation the angle α is set to 45°, the width w_1 to 5.0 mm and the height h to 17.5 mm. Next to the ratio of the tensile and the compressive stress condition, the maximum stress as well as the standard deviation of the stress levels are reviewed in order to avoid negative outliers in the final design. The resulting dimensions for the radii are $r_1 = 7.5$ mm, $r_2 = 3.0$ mm, $r_3 = 12.5$ mm and for the beam widths $w_2 = 4.5$ mm, $w_3 = 3.0$ mm. Table 1 provides an overview of the parameters varied along with variation ranges resulting dimensions.

The optimisation was made for a uniform material model over the entire specimen and therefore for an assumed equality between tensile and compressive properties. Since tensile and compressive

Table 1 Variation parameter and the resulting dimensions from the optimisation of the specimen geometry

Variation parameter	Variation range (mm)	Resulting dimension (mm)
r_1	7.5, 10.0, 12.5	7.5
r_2	2.5, 2.75, 3.0	3.0
r_3	10.0, 11.25, 12.5	12.5
w_2	4.5, 4.7, 4.9	4.5
w_3	2.9, 3.0, 3.1	3.0

properties can differ from each other, the resulting stress ratio of the compressive area to the tensile area is verified depending on the value of the moduli. The results are shown in Fig. 7.

A change of the moduli affects the tensile as well as the compressive stress condition both by a different magnitude. Hence, the stress conditions deviate from the desired equality. Especially with a low compressive modulus a change in each modulus has a high effect on the stress ratio. The results show that the desired uniformity is not generally valid. Consequently, with increasing deviation the time-dependent characteristic of the material has to be considered when comparing the moduli to each other. Furthermore, the result underlines the necessity of subsequent FE simulations in the testing concept since the state of stress is not independent of the other material properties and therefore cannot be predicted analytically.

The investigation is also done in dependence on the Poisson's ratio in Fig. 8.

Within the chosen variation range for the Poisson's ratio, the stress ratio varies by 0.002 at maximum. Compared to the Young's modulus the Poisson's ratio has a very low effect on the resulting stress ratio. A deviation between the tensile and compressive properties in this case has no significant influence on the strain rate within the specimen.

An important input parameter for the FE simulations is the actual geometry of the manufactured specimen. Since the geometry can differ from the defined nominal dimensions due to tolerances in milling, the influence of varying geometry parameters on the compressive modulus is studied. The results are shown in Fig. 9.

Within the chosen deviation range of ± 10% to the nominal dimension, the width of the compressive beam (w_3) in the centre of the specimen has the highest effect on the compressive modulus with a range of 540 MPa. Followed by the width of the tensile beam (w_1) with a range of 230 MPa. Since the resulting compressive modulus therefore depends on the exact dimensions of the specimen, they should be measured prior testing and considered for the subsequent FE simulations.

3.3 Experimental validation of the testing concept

For the validation of the new testing concept, five combined tensile compressive test specimens were manufactured and tested according to the defined

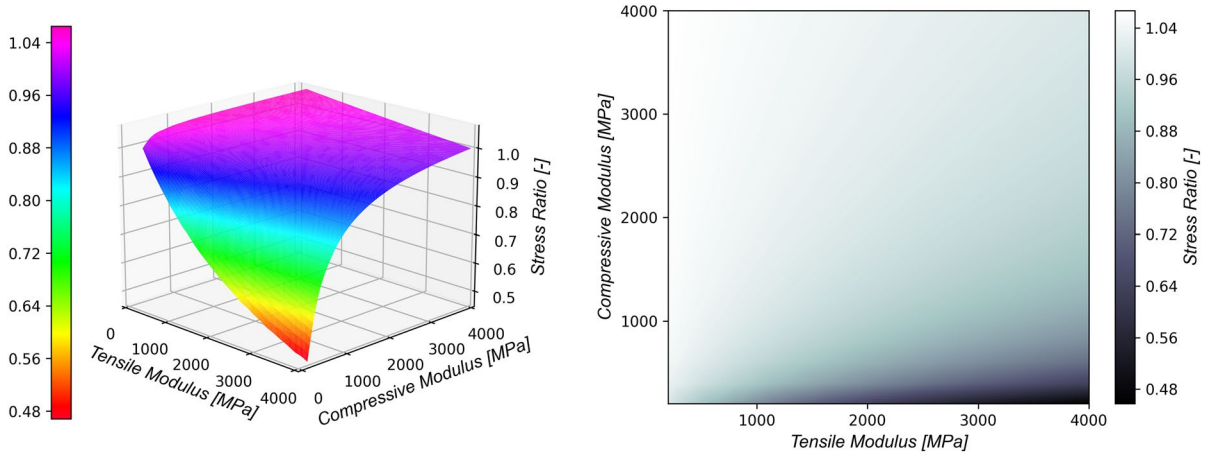

Fig. 7 Variation effect of tensile and compressive moduli on the stress ratio of compressive to tensile area

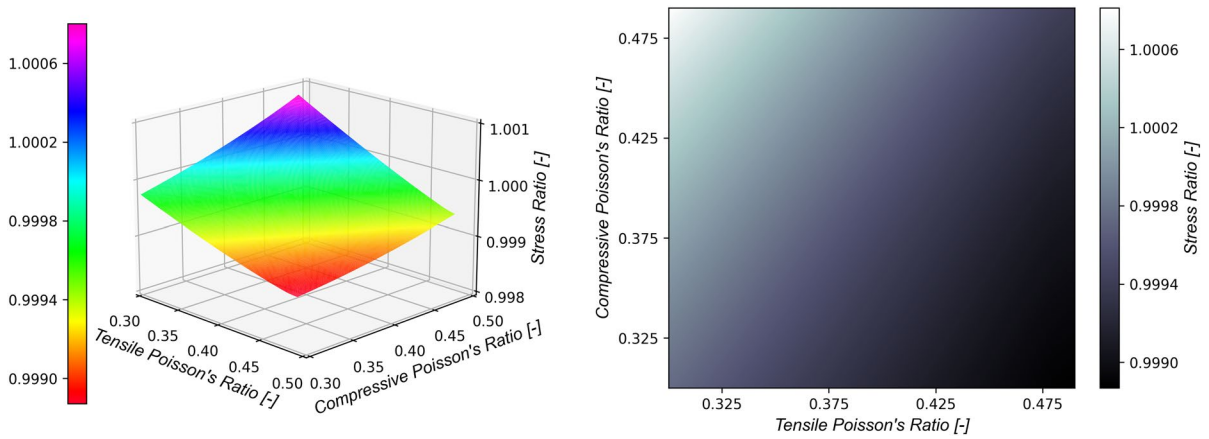

Fig. 8 Variation effect of tensile and compressive Poisson's ratio on the stress ratio of compressive to tensile area

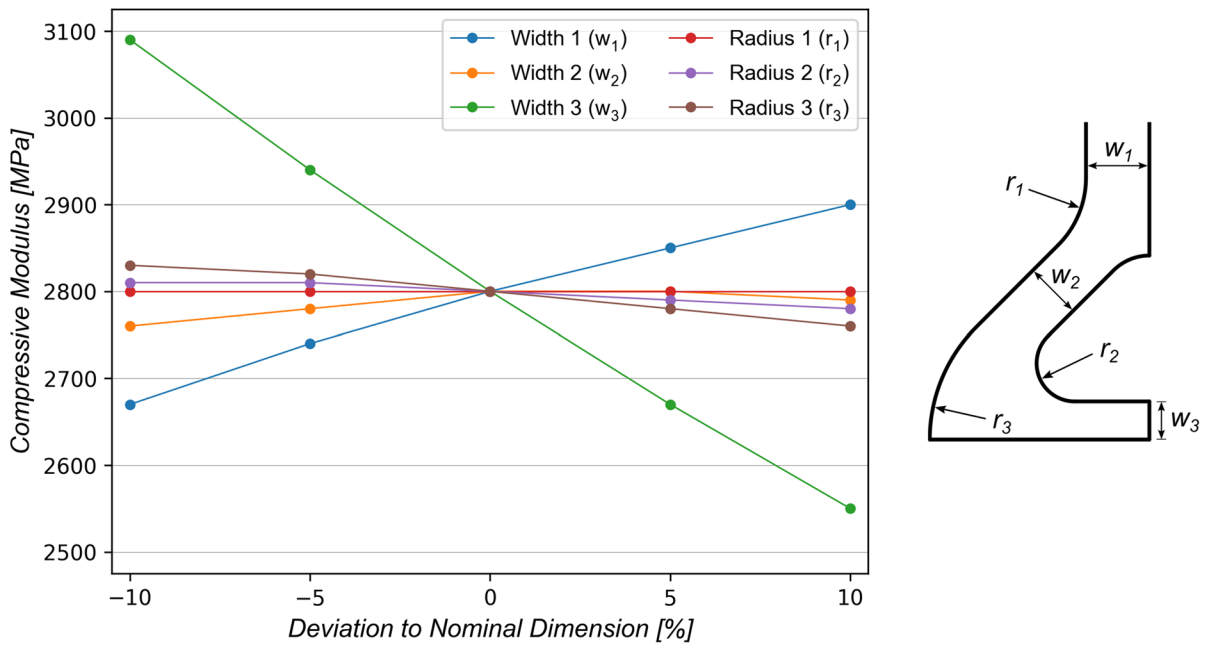

Fig. 9 Effect of geometric parameter variation of the combined tensile compressive test specimen on the compressive modulus according to the new testing concept

testing concept. Figure 10 shows the DIC measurement of the strain distribution including a histogram for strain values at the end of the evaluation time for one tested specimen.

The strain rates set for the single tensile and compressive tests are adjusted to the strain rates measured on the combined tensile compressive test specimen. The average value of the strain rate is 0.635%/min for the tensile area and 0.667%/min for the compressive area. Again, five tensile and compressive tests were carried out. The test results according to the new testing concept are compared to the references in Fig. 11.

The moduli determined with the new testing concept are higher than the reference values. In particular, the average tensile modulus is 4.1% and the average compressive modulus is 15.1% higher. In contrary,

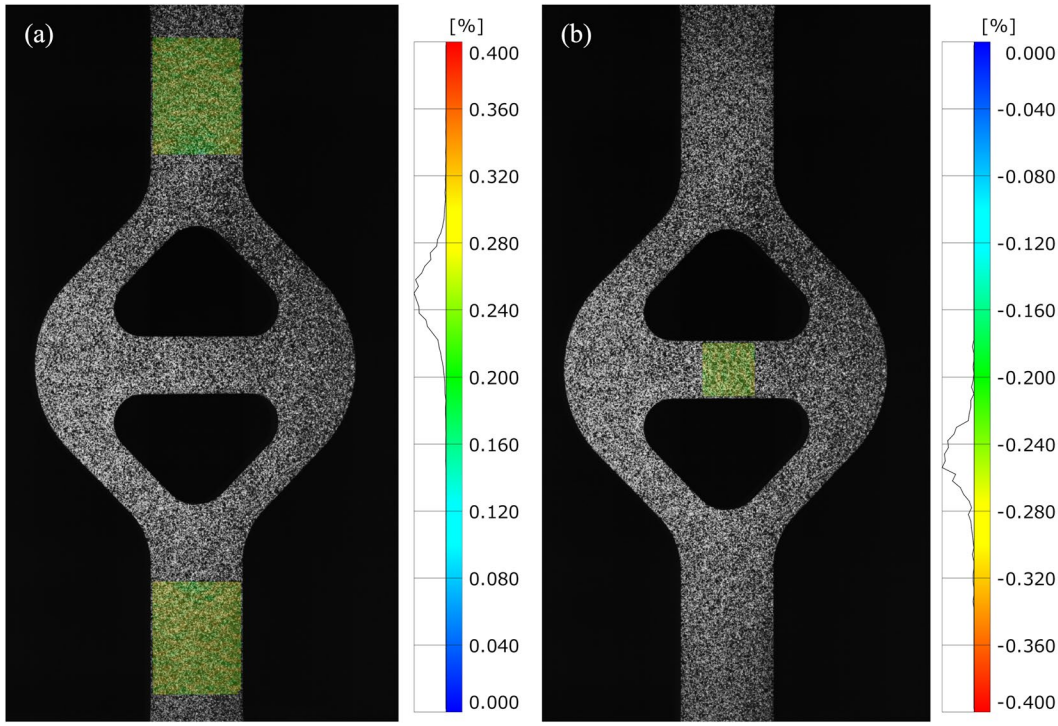

Fig. 10 DIC measurement of the strain distribution of a combined tensile compressive test specimen including a histogram for **a** the both evaluated tensile areas in y-direction at the average tension of 0.25% (with a standard deviation of 0.02% in both areas) and **b** the evaluated compressive area in x-direction at the average compression of 0.25% (with a standard deviation of 0.019%) to receive tensile modulus and tensile and compressive Poisson's ratio

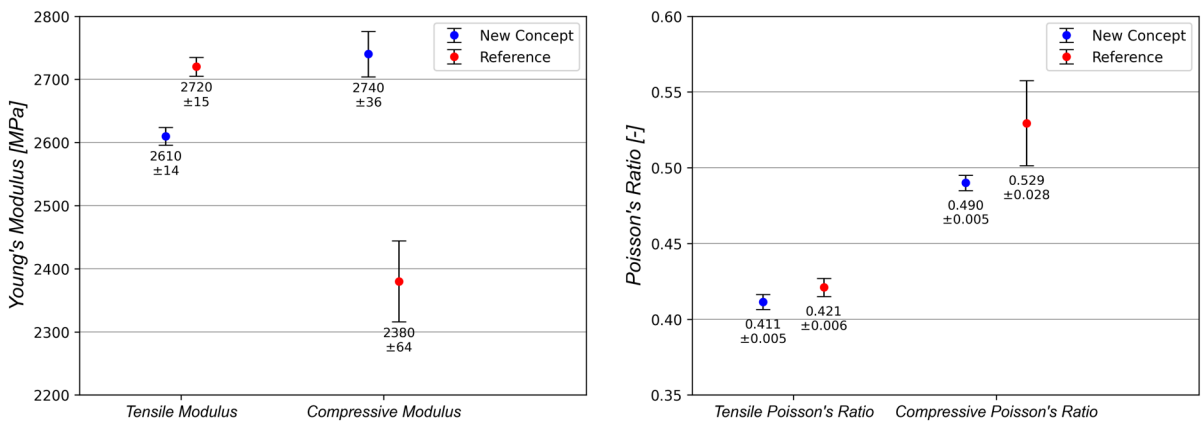

Fig. 11 Results of the experimental validation of the new testing concept; the error bars are calculated as the standard error of the mean

the measured Poisson's ratios are lower than the reference values. The tensile Poisson's ratio is 2.4% and the compressive Poisson's ratio is 7.4% lower. The results provided by the new testing concept are more robust since they have a lower standard error of the mean for all gained parameters.

The results indicate a good agreement for the tensile properties. The gap between the tensile moduli

can be explained by the testing temperature. Although the specimens were conditioned in a standard atmosphere according to ISO 29988-2 the tests could only be carried out in a non-climate-controlled room due to the location of the testing equipment needed. With an actual testing temperature of 24.4 °C, the temperature was around 4.7 °C lower for the comparative single tensile test which leads to a stiffer material behaviour. In addition to that, the small deviation in the tensile Poisson's ratio is seen to result from typical material fluctuations.

In contrast, the compressive properties reveal a larger gap. Most prominent, the reference value for the compressive Poisson's ratio is larger than 0.5 which indicates an increase in volume. In addition, the compressive modulus reveals a different trend in comparison to the tensile modulus. Since the reference value is about 90% of the tensile modulus and thus within the expected range, the new testing concept leads to a higher compressive stiffness of the material. One important cause for the deviation of both compressive parameters is the non-uniform compressive load on the reference specimen during testing. As mentioned, due to manufacturing tolerances of the specimen and the resulting sag in the stress strain diagram the measurement results needed to be post-processed. Therefore, the resulting parameters depend on the selected post-processing method. Furthermore, the specimens differ in their dimensions. While the compressive test specimen is $20 \times 10 \times 3$ mm^3, the compressive area in the combined tensile compressive test specimen is $12 \times 6 \times 3$ mm^3. Regarding the compressive Poisson's ratio only, the test setup solely enables the measurement of one transverse strain. In future work, an additional measurement of the second transverse strain could provide information about possible differences between both transverse strains for a better evaluation of the Poisson's ratio.

Another substantial impact on the resulting compressive modulus of the new testing concept is given by the material model chosen for the FE simulation. The specimen has been partitioned into two sections with separated tensile and compressive properties. Figure 12 presents the actual stress conditions of the specimen.

In the diamond-shaped area around the compressive partition, a superimposed stress condition occurs with biaxial tension, compression and shearing. However, the FE calculations in this area are only based on the tensile properties, which inevitably leads to a deviation from the calculated stress strain condition to the real material behaviour. This results in an error in the boundary conditions for the compressive area.

Unfortunately, Abaqus does not provide the possibility of implementing a linear elastic, asymmetric tensile and compressive material model. Consequently, the concept so far is just an approximation. For enhancing the testing concept, a user-defined material model needs to be developed and implemented, e.g. using UMAT.

The first step in extending the concept could therefore be programming the linear elastic, asymmetric tensile and compressive material model and implementing it for the entire body. This would also eliminate the necessity of partitioning the specimen into sections with different material properties. A subsequent validation of the enhanced concept will show whether the extension is sufficient. Otherwise, a further extension to include the shear modulus into the material model for the FE analysis would be necessary. This second enhancement is accompanied by the necessity of measuring the shear strain by DIC and implementing it as an additional loop in the optimisation algorithm. A benefit of the latter extension would be the possibility of obtaining the shear modulus as a further material parameter.

4 Conclusion

A new testing concept for the determination of Young's modulus and Poisson's ratio of tension and compression both in a single test was developed. Therefore, a new specimen geometry was designed where a homogeneous tensile stress as well as compressive stress condition occur in the same sample when tested in a universal testing machine. The experimental test accompanied by DIC provides the Poisson's ratios for tension and compression and the tensile modulus. For the determination of the compressive modulus, subsequent FE simulations are performed. The modulus is iteratively adjusted according to an optimisation algorithm programmed with Python in order to couple the simulated with the experimental compressive strain rate.

The testing concept is applied using the semi-crystalline thermoplastic polymer POM for validation purposes. Separate tensile and compressive

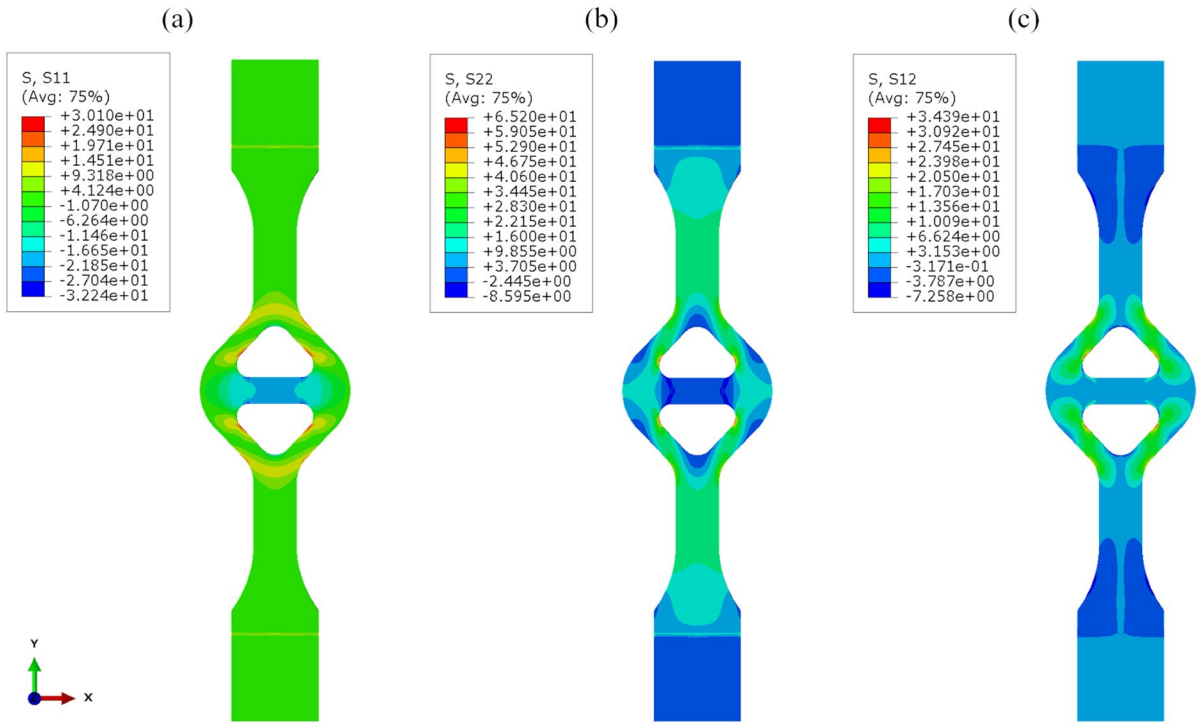

Fig. 12 Tensile and compressive stress condition in x-direction (**a**) and in y-direction (**b**) as well as shear stress condition in xy plane (**c**)

tests were performed to generate reference values for the four desired parameters. All values determined by this new method show good agreement with values measured in standard experiments at the same strain rate. However, the compressive modulus resulting from the new testing concept is approximately 15% higher than its reference value. The cause is mainly seen in the symmetric material model implemented for the FE simulation. Therefore, future work should start with the focus on deriving a material model with a full tension–compression asymmetry.

Acknowledgements The authors gratefully thank C. Schwab for inspiring discussions about different specimen geometries and the occurring stress conditions after loading.

Funding Open Access funding enabled and organized by Projekt DEAL. This research was funded by the Federal Ministry for Economic Affairs and Climate Action (BMWi) on the basis of a decision by the German Bundestag, grant number ZF4104911VS9.

Data availability The datasets generated and/or analysed during the current study are available from the corresponding author on reasonable request.

Declarations

Conflict of interest The authors have no competing interests to declare that are relevant to the content of this article.

References

Abanto-Bueno, J., Lambros, J.: Investigation of crack growth in functionally graded materials using digital image correlation. Eng. Fract. Mech. **69**(14–16), 1695–1711 (2002). https://doi.org/10.1016/S0013-7944(02)00058-9

Ali, H.B., Oleiwi, J.K., Othman, F.M.: Compressive and tensile properties of ABS material as a function of 3D printing process parameters. Rev. Compos. Matér. Avancés. **32**(3), 117–123 (2022). https://doi.org/10.18280/rcma.320302

Avril, S., Bonnet, M., Bretelle, A.-S., Grédiac, M., Hild, F., Ienny, P., Latourte, F., Lemosse, D., Pagano, S., Pagnacco, E., Pierron, F.: Overview of identification methods of mechanical parameters based on full-field measurements. Exp. Mech. **48**(4), 381–402 (2008). https://doi.org/10.1007/s11340-008-9148-y

Bing, P., Hui-min, X., Tao, H., Asundi, A.: Measurement of coefficient of thermal expansion of films using digital image correlation method. Polym. Test. **28**(1), 75–83 (2009). https://doi.org/10.1016/j.polymertesting.2008.11.004

Chaitat, S., Chantarapanich, N., Wanchat, S.: Effects of the 3DP process parameters on mechanical properties of polylactic acid part used for medical purposes. Rapid Prototyp J **28**(1), 143–160 (2022). https://doi.org/10.1108/RPJ-01-2021-0014

Grant, B.M.B., Stone, H.J., Withers, P.J., Preuss, M.: High-temperature strain field measurement using digital image correlation. J. Strain Anal. Eng. Des. **44**(4), 263–271 (2009). https://doi.org/10.1243/03093247JSA478

Grytten, F., Daiyan, H., Polanco-Loria, M., Dumoulin, S.: Use of digital image correlation to measure large-strain tensile properties of ductile thermoplastics. Polym. Test. **28**(6), 653–660 (2009). https://doi.org/10.1016/j.polymertesting.2009.05.009

He, T., Liu, L., Makeev, A., Shonkwiler, B.: Characterization of stress–strain behavior of composites using digital image correlation and finite element analysis. Compos. Struct. **140**, 84–93 (2016). https://doi.org/10.1016/j.compstruct.2015.12.018

Helfrick, M.N., Niezrecki, C., Avitabile, P., Schmidt, T.: 3D digital image correlation methods for full-field vibration measurement. Mech. Syst. Signal Process. **25**(3), 917–927 (2011). https://doi.org/10.1016/j.ymssp.2010.08.013

Kananathan, J., Samykano, M., Kadirgama, K., Ramasamy, D., Rahman, M.M.: Comprehensive investigation and prediction model for mechanical properties of coconut wood–polylactic acid composites filaments for FDM 3D printing. Eur. J. Wood Prod. **80**(1), 75–100 (2022). https://doi.org/10.1007/s00107-021-01768-1

Kim, K.-M., Shim, K.-B., Lum, C.: Predicting tensile and compressive moduli of structural lumber. Wood Fiber Sci. **43**(1), 83–89 (2011)

Lecompte, D., Smits, A., Sol, H., Vantomme, J., van Hemelrijck, D.: Mixed numerical–Experimental technique for orthotropic parameter identification using biaxial tensile tests on cruciform specimens. Int. J. Solids Struct. **44**(5), 1643–1656 (2007). https://doi.org/10.1016/j.ijsolstr.2006.06.050

Lin, Q., Labuz, J.F.: Fracture of sandstone characterized by digital image correlation. Int. J. Rock Mech. Min. Sci. **60**, 235–245 (2013). https://doi.org/10.1016/j.ijrmms.2012.12.043

Liu, L., Li, H., Li, X., Di, Wu., Zhang, G.: Underlying mechanisms of crack initiation for granitic rocks containing a single pre-existing flaw: insights from digital image correlation (DIC) analysis. Rock Mech. Rock Eng. **54**(2), 857–873 (2021). https://doi.org/10.1007/s00603-020-02286-x

Mazzanti, P., Caporossi, P., Muzi, R.: Sliding time master digital image correlation analyses of cubesat images for landslide monitoring: the Rattlesnake hills landslide (USA). Remote Sens. **12**(4), 592 (2020). https://doi.org/10.3390/rs12040592

Miao, S., Pan, P.-Z., Yu, P., Zhao, S., Shao, C.: Fracture analysis of Beishan granite after high-temperature treatment using digital image correlation. Eng. Fract. Mech. **225**, 106847 (2020). https://doi.org/10.1016/j.engfracmech.2019.106847

Moazzami, M., Ayatollahi, M.R., Akhavan-Safar, A.: Assessment of the fracture process zone in rocks using digital image correlation technique: the role of mode-mixity, size, geometry and material. Int. J. Damage Mech. **29**(4), 646–666 (2020). https://doi.org/10.1177/1056789519871334

Molimard, J.: Identification of the four orthotropic plate stiffnesses using a single open-hole tensile test. Exp. Mech. **45**(5), 404–411 (2005). https://doi.org/10.1177/0014485105057757

Mujika, F., Carbajal, N., Arrese, A., Mondragon, I.: Determination of tensile and compressive moduli by flexural tests. Polym. Test. **25**(6), 766–771 (2006). https://doi.org/10.1016/j.polymertesting.2006.05.003

Mutyala, R.S., Park, K., Günay, E.E., Kim, G., Lau, S., Jackman, J., Okudan Kremer, G.E.: Effect of FFF process parameters on mechanical strength of CFR-PEEK outputs. Int. J. Interact. Des. Manuf. **16**(4), 1385–1396 (2022). https://doi.org/10.1007/s12008-022-00944-8

Navaratnam, S., Ngo, T., Christopher, P., Linforth, S.: The use of digital image correlation for identifying failure characteristics of cross-laminated timber under transverse loading. Measurement **154**, 107502 (2020). https://doi.org/10.1016/j.measurement.2020.107502

Ngeljaratan, L., Moustafa, M.A.: Structural health monitoring and seismic response assessment of bridge structures using target-tracking digital image correlation. Eng. Struct. **213**, 110551 (2020). https://doi.org/10.1016/j.engstruct.2020.110551

Pan, Z., Huang, S., Su, Y., Qiao, M., Zhang, Q.: Strain field measurements over 3000 °C using 3D-digital image correlation. Opt. Lasers Eng. **127**, 105942 (2020). https://doi.org/10.1016/j.optlaseng.2019.105942

Pottier, T., Toussaint, F., Vacher, P.: Contribution of heterogeneous strain field measurements and boundary conditions modelling in inverse identification of material parameters. Eur. J. Mech. a. Solids **30**(3), 373–382 (2011). https://doi.org/10.1016/j.euromechsol.2010.10.001

Røhl, L., Larsen, E., Linde, F., Odgaard, A., Jørgensen, J.: Tensile and compressive properties of cancellous bone. J. Biomech. **24**(12), 1143–1149 (1991). https://doi.org/10.1016/0021-9290(91)90006-9

Rudawska, A., Frigione, M.: Effect of diluents on mechanical characteristics of epoxy compounds. Polymers (2022). https://doi.org/10.3390/polym14112277

Skarżyński, Ł: Mechanical and radiation shielding properties of concrete reinforced with boron-basalt fibers using digital image correlation and X-ray micro-computed tomography. Constr. Build. Mater. **255**, 119252 (2020). https://doi.org/10.1016/j.conbuildmat.2020.119252